# 6

## **Research Article**

Wenbo Ning\*, Wenjian Yang, Haoxian Wang, Kan Zhu, Yuhang Cai, Quanquan Yang and Qi Qi

# Swirling-annular-flow-induced instability of a micro shell considering Knudsen number and viscosity effects

https://doi.org/10.1515/phys-2025-0234 Received May 22, 2025; accepted October 13, 2025; published online November 26, 2025

**Abstract:** This paper investigates the instability of the outer thin-walled micro shell subjected to the swirling flowing fluid, where flowing fluid passes through the annular space formed by both inner and outer shells. The inviscid fluid hydrodynamic pressure and steady viscous forces are obtained respectively. The equations of motion are derived by the Hamilton's principle and solved with the zero-level contour and travelling-wave approaches. The impact of various parameters such as material parameters, fluid structure, fluid viscosity and Knudsen number, on the instability behaviors of this fluid-micro shell system is displayed. The findings of the research indicate that the elastic modulus is a prominent factor of affecting instability, and the shear couple forces  $\overline{\gamma}_{x\theta}$  have the most stabilizing effect leading to the increase of critical flow velocity by 14.454 %. The synergistic effect of the fluid viscosity and Knudsen number reduces the stability of such system by 80 %. The research contributes to understand the complex dynamical behaviors of fluid-conveying micro shell in design of micro devices including micromixer, microreactor, micro heat pipe.

**Keywords:** micro shell; annular flow; couple force; fluid viscosity; Knudsen number; modified couple stress theory

**Wenjian Yang, Haoxian Wang, Kan Zhu, Yuhang Cai and Qi Qi,** Faculty of Mechanical and Material Engineering, HuaiYin Institute of Technology, Huai'an, 223003, China

**Quanquan Yang**, Unmanned Aerial Vehicle Research Institute, HuaiYin Institute of Technology, Huai'an, 223003, China

# 1 Introduction

Shells/tubes/pipes containing flowing fluid inevitably experience dynamic forces generated by the flow. As a result, flow-induced vibration/instability phenomena are often found in many practical engineering and biological systems. For fluid-shell/tubes/pipes systems, their stability and dynamics are widely studied at macro scale level in the past few decades. Recently, microstructures like micro shells/tubes surrounding with fluid medium are the research hotspot due to their low power, super electromechanical properties. The size effect in microscale structures is intrinsic and inevitable. The traditional continuum mechanics cannot forecast size-dependent phenomenon in microstructures. For overcoming this size-dependent obstacle, certain high-order elasticity theories, including nonlocal elasticity theory/couple stress theory/nonlocal strain gradient theory [1-3], are proposed. One of these theories is Yang et al.'s modified couple stress theory [4]. Based on the Donnell's shell model, Zeighampour and Beni [5] analyzed vibrations of fluid-conveying double-walled carbon nanotube (DWCNT) through Differential Quadrature Method and the modified couple stress theory. It was found that due to the size effect, the stability region and nature frequency of the DWCNT would increase. The further studies indicated that the size effect remarkedly also affects the instability region of functionally graded materials (FGMs) micro shells [6]. Additionally, the volume fraction exponent, which stands for diverse component levels within FGMs, might be used to control vibration responses [7]. Dehrouyeh-Semnani et al. [8] conducted nonlinear analysis of the fluid-conveying micro-pipe using the modified couple stress theory. The key finding is that the nonlinear resonant behavior of the system is a hardening-type. Furthermore, the hardening behavior of system mostly be influenced by the slenderness ratio and the dimensionless mean flow velocity. The analysis was extended to the fluid-conveying porous functionally graded material pipes. The reference [9] examined the influences of the elastic foundation on nonlinear free and forced vibrations of the pipe. They found

<sup>\*</sup>Corresponding author: Wenbo Ning, Faculty of Mechanical and Material Engineering, HuaiYin Institute of Technology, Huai'an, 223003, China, E-mail: a3292472aowen@126.com

that the nonlinear frequency increases as the foundation stiffness grows. Norouzzadeh and Ansari [10] proposed the isogeometric analysis on small-scale shell-type structures for their nonlinear dynamic behaviors. It was found that the surface stress effects can influence the nonlinear configuration of amplitude-frequency. There are other studies conducted on fluid-filled nanotubes to analyze their wave propagation properties [11, 12]. It is found that the slip boundary affects the wave propagation inside them. The wave motions within nonhomogeneous carbon nanotubes conveying fluid were further studied and discussed the dispersion relation between the phase velocities and the fluid velocity [13, 14]. Dynamics and stability of microshell subjected to multi-loads have been studied recently. Wang et al. [15] reported the natural frequency responses and stability of fluid-conveying carbon nanotubes in the longitudinal magical field. The important phenomenon, the system would never lose stability at all when the magnetic field parameter is equal to or larger than the flow velocity, was found. Ansari and his coworkers analyzed single-walled boron nitride nanotubes (SWBNNTs) for the effects of thermal environments on their nonlinear vibration and flowinduced instability [16]. Their principal finding is that the frequency of SWBNNTs might increase with decrease of the temperature difference. Ansari et al. [16] further explored this similar issue within the thermal-magnetic field. Moreover, the synergistic effects induced by magnetic, electric, thermal and mechanical loadings are taken into consideration [17]. As discovered, the natural frequency of nano-beam depends on magneto-electro-thermo-mechanical coupling coefficient. Under the magnetic field, the impact of thermal radiation on the Casson flow past a vertical microchannel was discussed by Sreehari et al. [18], and Munjam et al. [19] analyzed the heat transport of a Casson liquid past a curved surface. The squeezing characteristics of the film lubricated by non-Newtonian fluids were studied by using the Rabinowitsch fluid model [20].

The non-slip boundary condition is always not reasonable to deal with fluid dynamics at micro scale. Therefore, the slip boundary condition must be considered. In slip flow regime, Thompson and Troian [21] presented a general boundary condition which overcomes shortcomings of the Navier's slip condition. The numeral calculations for determining of the relation of accommodation coefficients with slip length was performed by Wang et al. [22]. The detailed review on the experimental studies of slip boundary in Newtonian fluid was reported by Neto et al. [23].

With development of microfluidic devices and labon-a-chip technology, the annular flow has been often found in many engineering applications. For instance, the microreactors and micro heat pipes are subjected to an annular flow. When an annular flow has a circumferential flow velocity, the annular flow will be the swirling annular flow. To understand the stability of micro shells in annular fluid is of importance for design and manipulation of annular micromixers and micro-heat pipers. The stability of micro-pipes/tubes/shells subjected to an axial flow have attracted much investigation. However, there is few studies on the stability of same type structures under an annular swirling flow. Moreover, the different stabilizing effects of couple forces due to the material length-scale parameter are still undiscovered. The present study may be an effort to help fill part of this gap. Towards the purpose. The present word examines the effects of different coup forces and coupling effects of Kn number and fluid viscosity, on micro shell's dynamical behaviors, and give the physical explains. The proposed fluid-shell model cand guide the design of the micro devices.

# 2 Material and research method

# 2.1 The definition of the problem

The fluid-shell system can be observed from Figure 1. The two shells' density is  $\rho_s$ , elastic' modulus is E, Poission' ratio is v. The inner shell geometric parameters can be characterized by the length E, the wall thickness e and the radius e similarly, geometric characteristics of concentric outer shell include the length E, the wall thickness E0 and the radius E1. (Our) The system under consideration is located within the cylindrical coordinate system (E0; E1, E2, E3, with its origin E3 being left-sided and in the center of inner shell. The symbols E3, E4 and E5 represent axial, radical and circumferential directions, separately. The incompressible helical fluid (density E1) flows at the angular mean flow velocity E2 and the axial mean flow velocity E3.

This present paper is divided two parts: in the first part, the fluid is assumed be inviscid, with zero Kn number due to its relatively greater annular gap; in the second part, the fluid is viscous and non-zero Kn number for certain narrower annular flow.

# 2.2 Inviscid hydrodynamic pressure

The present fluid is assumed to be a potential flow due to its irrotation and non-viscosity. As is stated in literature [24], the hydrodynamic pressure (the hydrodynamic force) of the two coaxial shells can be expressed as [24]

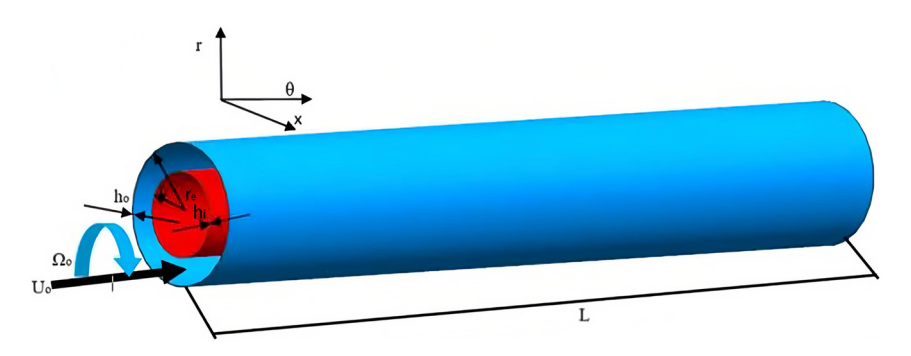


Figure 1: Geometry and coordinate of coaxial micro-shells under the swirling annular flow.

$$p_{i} = -\frac{\rho_{f}}{N} \left( \frac{\partial}{\partial t} + \frac{V_{o}}{r} \frac{\partial}{\partial \theta} + U_{o} \frac{\partial}{\partial x} \right)^{2} \left\{ \left[ I_{j}(\lambda r_{i}) K'_{j}(\lambda r_{o}) - I'_{j}(\lambda r_{o}) K_{j}(\lambda r_{i}) \right] w_{i} + \left[ I'_{j}(\lambda r_{i}) K_{j}(\lambda r_{i}) - I_{j}(\lambda r_{i}) K'_{j}(\lambda r_{i}) \right] w_{o} \right\}$$

$$(1a)$$

$$p_{o} = -\frac{\rho_{f}}{N} \left( \frac{\partial}{\partial t} + \frac{V_{o}}{r} \frac{\partial}{\partial \theta} + U_{o} \frac{\partial}{\partial x} \right)^{2} \left\{ \left[ I_{j}(\lambda r_{o}) K'_{j}(\lambda r_{o}) - I'_{j}(\lambda r_{o}) K_{j}(\lambda r_{o}) \right] w_{i} + \left[ I'_{j}(\lambda r_{i}) K_{j}(\lambda r_{o}) - I_{j}(\lambda r_{o}) K'_{j}(\lambda r_{i}) \right] w_{o} \right\}$$
(1b)

in which  $N = I'_i(\lambda r_i)K'_i(\lambda r_o) - I'_i(\lambda r_o)K'_i(\lambda r_i)$ , the tangential mean velocity of annular flow  $V_o = \Omega_o \times r$ .

Symbols i, o denote inner and outer shells, separately;  $I_i$ ,  $K_i$  are the j order modified Bessel functions for the first and second kinds, separately;  $\lambda$  presents the order of axial vibration model; the symbols ' is the differentiation operation;  $w_{i/o}$  indicates r-direction

When either inner or outer shell is perfect stiff, the expression (1) might be reformulated [24]. Thus,

$$p_{i} = -\frac{\rho_{f}}{\Gamma} \left( \frac{\partial}{\partial t} + \frac{V_{o}}{r} \frac{\partial}{\partial \theta} + U_{o} \frac{\partial}{\partial x} \right)^{2} \left[ I_{j} (\lambda r_{i}) K'_{j} (\lambda r_{o}) - I'_{j} (\lambda r_{o}) K_{j} (\lambda r_{i}) \right] w_{i}$$
(2a)

$$p_{o} = -\frac{\rho_{f}}{\Gamma} \left( \frac{\partial}{\partial t} + \frac{V_{o}}{r} \frac{\partial}{\partial \theta} + U_{o} \frac{\partial}{\partial x} \right)^{2} \left[ I'_{j} (\lambda r_{i}) K_{j} (\lambda r_{o}) - I_{j} (\lambda r_{o}) K'_{j} (\lambda r_{i}) \right] w_{o}$$
(2b)

# 2.3 The governing equations of motion

In contrast with the conventional couple stress theory, Yang et al.'s [4] modified couple stress theory is extensively

adopted due to its symmetry and compaction. The strain energy in volume  $\Omega$  can be defined by [4]

$$U_{e} = \frac{1}{2} \int_{\Omega} \left( \sigma_{ij} \varepsilon_{ij} + m_{ij} \chi_{ij} \right) dv$$
 (3)

in which  $\sigma_{ij}$ ,  $\varepsilon_{ij}$ ,  $m_{ij}$  and  $\chi_{ij}$  represent respectively the stress tensor, Cauchy strain tensor, the higher order stress tensor, the symmetric rotation gradient tensor;  $i, j = x, \theta, r$ . These tensors are presented by [25]

$$\varepsilon_x = u_x + zk_x = \frac{\partial u}{\partial x} + zk_x,$$
 (4a)

$$\varepsilon_{\theta} = u_{\theta} + zk_{\theta} = \frac{\partial v}{r\partial \theta} + \frac{w}{r} + zk_{\theta},$$
 (4b)

$$\varepsilon_{x\theta} = u_{x\theta} + 2zk_{x\theta} = \frac{\partial u}{r\partial\theta} + \frac{\partial v}{\partial x} + 2zk_{x\theta}$$
 (4c)

$$k_{x} = -\frac{\partial^{2} w}{\partial x^{2}}, k_{\theta} = -\frac{\partial^{2} w}{r^{2} \partial \theta^{2}}, k_{x\theta} = -\frac{\partial^{2} w}{r \partial x \partial \theta}$$
 (5)

with u, v and w representing shell displaces at x-,  $\theta$ -, and r-directions separately;  $k_{\scriptscriptstyle X},\,k_{\scriptscriptstyle heta}$  and  $k_{\scriptscriptstyle X heta}$  represent the shell's curvatures and twist; z indicates a displace variable of rdirection.

The shell's internal force and moment resultants is shown in the matrix.

$$N_{x} = \frac{E_{1}}{1 - v^{2}} u_{x} + \frac{vE_{1}}{1 - v^{2}} u_{\theta};$$

$$N_{\theta} = \frac{vE_{1}}{1 - v^{2}} u_{x} + \frac{E_{1}}{1 - v^{2}} u_{\theta};$$

$$N_{x\theta} = \frac{E_{1}}{2(1 + v)} u_{x\theta};$$

$$M_{x} = \frac{E_{2}}{1 - v^{2}} k_{x} + \frac{vE_{2}}{1 - v^{2}} k_{\theta};$$

$$M_{x} = \frac{vE_{2}}{1 - v^{2}} k_{x} + \frac{E_{2}}{1 - v^{2}} k_{\theta};$$

$$M_{x} = \frac{E_{2}}{1 - v^{2}} k_{x\theta}.$$
(6b)

in which  $\{E_1, E_2\} = \int_{-\frac{h}{2}}^{\frac{h}{2}} E(1, z^2) dz$ .

According to the relation of higher order stress tensor with symmetric rotation gradient tensor  $m_{ij}=2G\chi_{ij}$  [4], through the integration calculation, one obtains

$$m_{x} = \frac{El^{2}h}{2(1+v)} \chi_{x}; m_{\theta} = -\frac{El^{2}h}{4(1+v)} \chi_{\theta};$$

$$m_{x\theta} = \frac{El^{2}h}{2(1+v)} \chi_{x\theta}; m_{xz} = \frac{El^{2}h}{4(1+v)} \chi_{xz};$$

$$m_{\theta z} = \frac{El^{2}h}{4(1+v)} \chi_{\theta z}.$$
(7)

in which  $\kappa = \frac{El^2h}{2(1+v)}$ ,  $G = \frac{E}{2(1+v)}$ , l is the material length-scale parameter;  $\chi_{\rm x} = \frac{1}{2} \frac{\partial^2 w}{r \partial x \partial \theta}$ ,  $\chi_{\theta} = -\frac{1}{2} \frac{\partial^2 w}{r \partial x \partial \theta}$ ,  $\chi_{x\theta} = \frac{1}{2} \left( \frac{\partial^2 w}{r^2 \partial \theta^2} - \frac{\partial^2 w}{\partial x^2} \right)$ ,  $\chi_2 = 0$ ,  $\chi_{\rm xz} = \frac{1}{4} \left( \frac{\partial^2 v}{\partial x^2} - \frac{\partial^2 u}{r^2 \partial \theta^2} \right)$ ,  $\chi_{\theta z} = \frac{1}{4} \left( \frac{\partial^2 v}{r \partial x \partial \theta} - \frac{\partial^2 u}{r^2 \partial \theta^2} \right)$ .

Based on the Hamilton principle, the shell's motion equations were given.

$$\int_{0}^{T} \delta(T + W - U_{\rm e}) dt = 0$$
 (8)

in which  $\delta$  stands for the variational operator, T represents the kinetic energy,  $U_{\rm e}$  suggests the stain energy while W indicates the work on shell wall made by hydrodynamic load.

The stain energy can be obtained by integrating

$$\delta U_{\rm e} = \int_{0}^{L} \int_{0}^{2\pi} \int_{-\frac{h}{2}}^{\frac{h}{2}} \left( \sigma_{\chi} \delta \varepsilon_{\chi} + \sigma_{\theta} \delta \varepsilon_{\theta} + \sigma_{\chi \theta} \delta \varepsilon_{\chi \theta} \right) \mathrm{d}\chi \mathrm{d}\theta \mathrm{d}z$$

$$+ \int_{0}^{L} \int_{0}^{2\pi} \int_{-\frac{h}{2}}^{\frac{h}{2}} \left( m_{\chi} \delta \chi_{\chi} + m_{\theta} \delta \chi_{\theta} + m_{\chi \theta} \delta \chi_{\chi \theta} \right)$$
(9)

$$+ m_{xz} \delta \chi_{xz} + m_{\theta z} \delta \chi_{\theta z} dx d\theta dz$$

with the kinetic energy being determined by

$$\delta T = \rho_s h \int_0^L \int_0^{2\pi} \left[ \frac{\partial u}{\partial t} \delta \left( \frac{\partial u}{\partial t} \right) + \frac{\partial v}{\partial t} \delta \left( \frac{\partial v}{\partial t} \right) + \frac{\partial w}{\partial t} \delta \left( \frac{\partial w}{\partial t} \right) \right] dx d\theta$$
(10)

The hydrodynamic load-made work is presented below

$$\delta W = \int_{0}^{L} \int_{0}^{2\pi} p_{i/o} \delta w dx d\theta$$
 (11)

where  $p_{i/o}$  stands for the hydrodynamic force and is acquired in subsection 2.2.

When Eqs. (9)–(11) are substituted in Eq. (8), the shell conveying fluid's motion equations can be generated by some mathematical manipulations, as shown below [26]:

$$\frac{\partial N_x}{\partial x} + \frac{1}{r} \frac{\partial N_{\theta x}}{\partial \theta} + \frac{1}{2} \frac{\partial^2 Y_{xz}}{r \partial x \partial \theta} + \frac{1}{2} \frac{\partial^2 Y_{\theta z}}{r^2 \partial \theta^2} = \rho_s \frac{\partial^2 u}{\partial t^2}$$
 (12a)

$$\frac{\partial N_{x\theta}}{\partial x} + \frac{1}{r} \frac{\partial N_{\theta}}{\partial \theta} - \frac{1}{2} \frac{\partial^2 Y_{xz}}{\partial x^2} - \frac{1}{2} \frac{\partial^2 Y_{\theta z}}{r \partial x \partial \theta} = \rho_s \frac{\partial^2 v}{\partial t^2}$$
 (12b)

$$\frac{\partial^{2} M_{x}}{\partial x^{2}} + \frac{1}{r} \frac{\partial^{2} M_{x\theta}}{\partial x \partial \theta} + \frac{1}{r} \frac{\partial^{2} M_{\theta x}}{\partial x \partial \theta} - \frac{N_{\theta}}{r} - \frac{1}{r} \frac{\partial^{2} Y_{x}}{\partial x \partial \theta} + \frac{1}{r} \frac{\partial^{2} Y_{\theta}}{\partial x^{2}} - \frac{1}{2} \frac{\partial^{2} Y_{x\theta}}{\partial r^{2} \partial \theta^{2}} + \frac{1}{2} \frac{\partial^{2} Y_{x\theta}}{\partial x^{2}} = \rho_{s} \frac{\partial^{2} W}{\partial t^{2}} + p_{i/o}$$
(12c)

After forces, couple stress and moments are introduced in Eqs. (12), the shell's motion equations are obtained in the linear matrix operator

$$\zeta \begin{bmatrix} u_{i/o} \\ v_{i/o} \\ w_{i/o} \end{bmatrix} = \begin{bmatrix} 0 \\ 0 \\ p_{i/o} \end{bmatrix}$$
(13)

where 
$$\zeta = \frac{E_1}{1-v^2} \begin{bmatrix} \zeta_{11} & \zeta_{12} & \zeta_{13} \\ \zeta_{21} & \zeta_{22} & \zeta_{23} \\ \zeta_{31} & \zeta_{32} & \zeta_{33} \end{bmatrix}$$

$$\zeta_{11} = \frac{\partial^2}{\partial x^2} + \frac{1-v}{2r^2} \frac{\partial^2}{\partial \theta^2} - l^2 \frac{1-v}{2r^2} \frac{\partial^4}{\partial x^2 \partial \theta^2}$$

$$\zeta_{11} = \frac{\partial}{\partial x^2} + \frac{1}{2r^2} \frac{\partial}{\partial \theta^2} - l^2 \frac{1}{2r^2} \frac{\partial}{\partial x^2 \partial \theta^2} - l^2 \frac{1}{2r^2} \frac{\partial}{\partial x^2 \partial \theta^2} - l^2 \frac{1-v}{2r^4} \frac{\partial}{\partial \theta^4} - \rho_s \frac{1-v^2}{E} \frac{\partial^2}{\partial t^2},$$

$$\zeta_{12} = \zeta_{21} = \frac{1+v}{2r} \frac{\partial^2}{\partial x \partial \theta} + l^2 \frac{1-v}{2r} \frac{\partial^4}{\partial x^3 \partial \theta} + l^2 \frac{1-v}{2r} \frac{\partial^4}{\partial x^3 \partial \theta}$$
$$+ l^2 \frac{1-v}{2r^3} \frac{\partial^4}{\partial x \partial \theta^3}, \zeta_{13} = \zeta_{31} \frac{v}{r} \frac{\partial}{\partial y},$$

$$\begin{split} \zeta_{22} &= \frac{1-\upsilon}{2} \frac{\partial^{2}}{\partial x^{2}} + \frac{1}{r} \frac{\partial^{2}}{\partial \theta^{2}} - l^{2} \frac{1-\upsilon}{2} \frac{\partial^{4}}{\partial x^{4}} \\ &- l^{2} \frac{1-\upsilon}{2r^{2}} \frac{\partial^{4}}{\partial x^{2} \partial \theta^{2}} - \rho_{s} \frac{1-\upsilon^{2}}{E} \frac{\partial^{2}}{\partial t^{2}}, \zeta_{23} = \zeta_{32} = \frac{\upsilon}{r^{2}} \frac{\partial}{\partial \theta}, \\ \zeta_{33} &= \frac{1}{r^{2}} + \frac{h^{2}}{12} \Delta \Delta + \rho_{s} \frac{1-\upsilon^{2}}{E} \frac{\partial^{2}}{\partial t^{2}} + l^{2} \frac{1-\upsilon}{2} \frac{\partial^{4}}{\partial x^{4}} \\ &+ l^{2} \frac{1-\upsilon}{2r^{4}} \frac{\partial^{4}}{\partial \theta^{4}} + l^{2} \frac{1-\upsilon}{2r^{2}} \frac{\partial^{4}}{\partial x^{2} \partial \theta^{2}}. \end{split}$$

in which  $\Delta = \frac{\partial^2}{\partial x^2} + \frac{1}{r^2} \frac{\partial^2}{\partial \theta^2}$ .

# 2.4 Method of solution

It has been proved that the travelling-wave type solution used for the stability analysis of fluid-filled shells is validity

[27]. By expanding the displace components as travellingwave, the displaces u, v and w for either inner or outer shell under simply supported boundary conditions are presented in [27].

$$\begin{bmatrix} u_{i/o} \\ v_{i/o} \\ w_{i/o} \end{bmatrix} = \begin{bmatrix} u_{mn} \exp[-i(\lambda x + n\theta - \omega t)] \\ v_{mn} \exp[-i(\lambda x + n\theta - \omega t)] \\ w_{mn} \exp[-i(\lambda x + n\theta - \omega t + \pi/2)] \end{bmatrix}$$

$$\times \left(\lambda = \frac{m\pi}{L}\right)$$
(14)

The motion equations will be nondimensionalized by introducing the reference time  $\tau$ . Given below:

$$\tau = r_i \sqrt{\frac{\rho_s (1 - v^2)}{E}}$$

and leading to

$$\overline{l} = \frac{l}{r_i}, \overline{t} = \frac{t}{\tau}, \overline{h} = \frac{h}{r_i}, \overline{x} = \frac{x}{r_i}, \overline{L} = \frac{L}{r_i}, \overline{r} = \frac{r}{r_i},$$

$$\overline{p} = \frac{\tau^2}{\rho_s r_i^2} p, \overline{U_o} = \frac{U_o \tau}{r_i},$$

$$\overline{V_o} = \frac{V_o \tau}{r_i}, \lambda_c = \frac{r_o}{r_i}, k = \frac{r_o - r_i}{r_i}, \overline{\omega} = \omega \tau,$$

$$\begin{bmatrix} \overline{u_{i/o}} \\ \overline{v_{i/o}} \\ \overline{w_{i/o}} \end{bmatrix} = \frac{1}{r_i} \begin{bmatrix} u_{i/o} \\ v_{i/o} \\ w_{i/o} \end{bmatrix}.$$
(15)

In the case of the elastic outer shell and perfect rigid inner shell, based on Eq. (2b) and Eq. (15), dimensionless form of Eq. (13) can be acquired:

$$\zeta \mathbf{u} = \zeta \begin{bmatrix} \overline{u_o} \\ \overline{v_o} \\ -i\overline{w_o} \end{bmatrix} = \begin{bmatrix} 0 \\ 0 \\ 0 \end{bmatrix}$$
 (16)

where 
$$\zeta = \begin{bmatrix} \zeta_{11} & \zeta_{12} & \zeta_{13} \\ \zeta_{21} & \zeta_{22} & \zeta_{23} \\ \zeta_{31} & \zeta_{32} & \zeta_{33} \end{bmatrix}$$

$$\zeta_{11} = -\lambda^2 - \frac{1-\upsilon}{2\lambda_c^2} n^2 - \overline{l}^2 \frac{1-\upsilon}{4\lambda_c^2} \lambda^2 n^2 - \overline{l}^2 \frac{1-\upsilon}{4\lambda_c^4} n^4 + \overline{\omega}^2,$$

$$\zeta_{12} = \zeta_{21} = \frac{1+\upsilon}{2\lambda_c} \lambda n + \bar{l}^2 \frac{1-\upsilon}{4\lambda_c} \lambda^3 n + \bar{l}^2 \frac{1-\upsilon}{4\lambda_c^3} \lambda n^3,$$
  
$$\zeta_{13} = \zeta_{31} = -\frac{i\upsilon\lambda}{\lambda_c},$$

$$\begin{split} \zeta_{22} &= -\frac{1-\upsilon}{2}\lambda^2 - \frac{n^2}{\lambda_c^2} + \overline{\omega}^2 - \frac{1-\upsilon}{4}\overline{l}^2\lambda^4 - \frac{1-\upsilon}{4\lambda_c^2}\overline{l}^2\lambda^2n^2, \\ \zeta_{22} &= \zeta_{32} - \frac{\upsilon}{\lambda^2}in, \end{split}$$

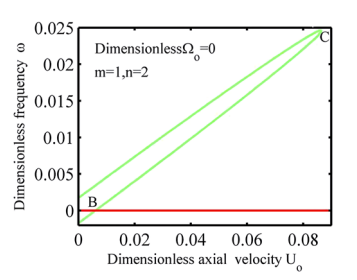


Figure 2: Judgment criterion of instability from curve of dimensionless frequency against dimensionless axial flow velocity.

$$\begin{split} \zeta_{33} &= \frac{1}{\lambda_c^2} + \frac{\overline{h}^2}{12} \left( \lambda^2 + \frac{n^2}{\lambda_c^2} \right)^2 + \overline{l}^2 \frac{1 - \upsilon}{4^2} \lambda^4 + \overline{l}^2 \frac{1 - \upsilon}{4\lambda_c^4} n^4 \\ &+ \overline{l}^2 \frac{3(1 - \upsilon)}{2\lambda_c^2} \lambda^2 n^2 - \overline{\omega}^2 - \frac{\overline{\Gamma}_2}{\overline{\Gamma}} \frac{1}{\overline{h}} \frac{\rho_f}{\rho_s} \left( \overline{\omega} - \lambda \overline{U_o} - n \frac{\overline{V_o}}{\lambda_c} \right)^2. \end{split}$$

here  $\overline{\Gamma} = I'_n(\lambda)K'_n(\lambda\lambda_c) - I'_n(\lambda\lambda_c)K'_n(\lambda), \overline{\Gamma_2} = I'_n(\lambda)K_n(\lambda\lambda_c) - I_n(\lambda\lambda_c)K'_n(\lambda).$ 

Considering non-zero solutions in Eq. (15),

$$|\zeta| = 0 \tag{17}$$

By mathematical operations, Eq. (17) represents the 6order polynomial of dimensionless frequency variable on its left side, with two fluid velocities being two parameters. The close curve, which represents the dispersion relation  $\overline{\omega} - \overline{U}_o(\overline{V}_o)(\overline{V}_o/\overline{U}_o)$  is given), will be obtained by the aid of the function 'ezplot' in MATLAB. Based on these feature points of the contour curve drawn by software MAT-LAB, critical flow velocities associated to the corresponding modes are obtained. This is called 'the zero-level contour method', which may obtain the results directly by drawing "the close curve" by the aid of the software package MATLAB. From the zero-level contour method, the judgment criterion of instability is given below:

When the backward wave crosses the zero-frequency line at point B, the system loses stability by divergence, as shown Figure 2. When the forward and backward travelling frequencies coalesce at point C, the point can be considered to represent the form of the coupled-mode flutter of the system.

# 3 Results and discussion

# 3.1 Validation of the present method

Little research is conducted to analyze the micro-shell stability under an annular flow in published literatures. So, it is difficult to exactly compare our results with existing findings. To evaluate accuracy and reasonableness of 'zero-level contour method', the annular flow is simplified into internal flow inside the micro-shell at the axial velocity. Corresponding material and geometric parameters of micro-shell under simply supported conditions are observed below [26].

$$L = 100 \ \mu\text{m}, r = 10 \ \mu\text{m}, h = 0.1 \ \mu\text{m};$$
 
$$E = 1.44 \times 10^{11} \ P_{\text{a}}, v = 0.38, \rho_{\text{s}} = 1{,}000 \ \text{kgm}^{-3},$$
 
$$\rho_{\text{f}} = 1{,}000 \ \text{kgm}^{-3}, l = 17.6 \ \mu\text{m}.$$

It should to be noticed that the internal fluid-exerted hydrodynamic pressure on the shell's inner wall is determined by

$$p_i^i = -\rho_f \frac{L}{m\pi} \frac{I_n(\lambda)}{I_n'(\lambda)} \left( \frac{\partial}{\partial t} + U_o \frac{\partial}{\partial x} \right) w \tag{18}$$

Thus, the entries  $\zeta_{ij}$  within matrix  $\zeta$  can be presented as

$$\begin{split} \zeta_{11} &= -\lambda^2 - \frac{1-\upsilon}{2} n^2 - \overline{l}^2 \frac{1-\upsilon}{4} \lambda^2 n^2 - \overline{l}^2 \frac{1-\upsilon}{4} n^4 + \overline{\omega}^2, \\ \zeta_{12} &= \zeta_{21} = \frac{1+\upsilon}{2} \lambda n + \overline{l}^2 \frac{1-\upsilon}{4} \lambda^3 n + \overline{l}^2 \frac{1-\upsilon}{4} \lambda n^3, \\ \zeta_{13} &= \zeta_{31} = -i\upsilon\lambda, \\ \zeta_{22} &= -\frac{1-\upsilon}{2} \lambda^2 - n^2 + \overline{\omega}^2 - \overline{l}^2 \frac{1-\upsilon}{4} \lambda^4 - \frac{1-\upsilon}{4} \overline{l}^2 \lambda^2 n^2, \\ \zeta_{22} &= \zeta_{32} - \upsilon \text{in}, \\ \zeta_{33} &= 1 + \frac{\overline{h}^2}{12} (\lambda^2 + n^2)^2 + \overline{l}^2 \frac{1-\upsilon}{4^2} \lambda^4 + \overline{l}^2 \frac{1-\upsilon}{4} n^4 \\ &+ \overline{l}^2 \frac{3(1-\upsilon)}{2} \lambda^2 n^2 - \overline{\omega}^2 - \frac{\overline{L}}{m\pi} \frac{\overline{I}_n(\lambda)}{\overline{I}'_n(\lambda)} \frac{1}{\overline{h}} \\ &\times \frac{\rho_f}{a} \left( \overline{\omega} - \lambda \overline{U_o} \right)^2. \end{split}$$

When the aforementioned zero-level contour method is used, dimensionless velocities with/without the size scale effect can be translated into dimensional results (Table 1) and later compared to Zhou and Wang's findings [26].

As discovered, the maximum error of 5.91 % is detected. Therefore, our critical flow velocities well conform to the reported ones [26]. Furthermore, the material length-scale parameter renders significantly increased critical

axial velocities relative to the classical theory-obtained counterparts.

# 3.2 Dynamical stability analysis

The present work just considers the perfect stiff inner shell and elastic outer shell and analyzes size-dependent stability of a micro-shell in the annular fluid involving axial and/or circumferential velocities. The micro-shell's dynamic behaviors are analyzed under simply supported boundary conditions. While boundary conditions in two edges x = 0, L can be presented as displaces.

$$v_{i/o} = w_{i/o} = 0$$
 (19a)

$$r_{i/o}\frac{\partial u_{i/o}}{\partial x} + v\frac{\partial v_{i/o}}{\partial \theta} + v\omega_{i/o} - \frac{h_{i/o}^2}{12}\frac{\partial^2 w_{i/o}}{\partial x^2} = 0$$
 (19b)

$$r_{i/o}^2 \frac{\partial^2 w_{i/o}}{\partial x^2} + v \frac{\partial^2 w_{i/o}}{\partial \theta^2} - v \frac{\partial v_{i/o}}{\partial \theta} - r_{i/o} \frac{\partial u_{i/o}}{\partial x} = 0$$
 (19c)

For easy to compare, geometric parameters below are adopted.

$$L = 100 \text{ } \mu\text{m}, r_0 = 10 \text{ } \mu\text{m}, k = \frac{r_0 - r_i}{r_i},$$

$$r_i = 9.0901 \ \mu \text{m}(k = 0.1), h = h_i = h_o = 0.1 \ \mu \text{m}.$$

The material properties in the calculations are chosen

$$E = 1.44 \times 10^{11} P_a$$
,  $v = 0.38$ ,  $ρ_s = 1,000 \text{ kgm}^{-3}$ ,  
 $ρ_f = 1,000 \text{ kgm}^{-3}$ ,  $l = h = 0.1 \text{ μm}$ .

First, the zero-level contour method is utilized for calculating flow velocity related to diverse models (m, n) by solving Eq. (19). From the obtained results, the smallest flow velocity for stability loss and the corresponding mode are found, as shown in Figure 2. From the judgment criterion of stability loss, the backward travelling wave intersects with the zero-frequency line at point B ( $\overline{U_o}=0.006012$ ), which represents that system stability is lost in the form of divergence. After the forward travelling frequency coalesces with backward one at 'nose' point C, this point stands for the system's coupled-mode flutter form.

Similarly, for fluid flow having just angular velocity component, similar results are acquired with zero-level contour method based on judgment criteria of stability loss. It

Table 1: Comparisons of critical axial velocities instability by divergence for a simply supported micro-shell.

	Modified couple stress theory		Class continuum mechanics theory	
<i>U<sub>o</sub></i> (m/s)	84.5571 [26]	85.7612 (present)	14.8067 [26]	13.9315 (present)
Mode ( <i>m</i> , <i>n</i> )	(1, 0)	(3, 1)	(1, 2)	(1, 1)

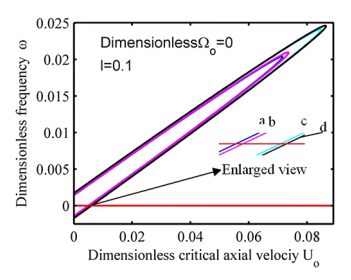


**Figure 3:** Variation of the dimensionless frequency with the dimensionless axial flow velocity: (a) Without considering all couple forces  $\overline{\gamma}_{ij}(\overline{U}_o=0.004975)$ ; (b) without considering shear couple forces  $\overline{\gamma}_{x\theta}, \overline{\gamma}_{xz}, \overline{\gamma}_{\theta z}(\overline{U}_o=0.005121)$ ; (c) without considering normal couple forces  $\overline{\gamma}_x, \overline{\gamma}_{\theta}(\overline{U}_o=0.005889)$ ; (d) with considering all couple forces  $\overline{\gamma}_{ij}(\overline{U}_o=0.006012)$ .

is found that critical angular velocity due to divergence is  $\overline{\Omega_o}=0.008576$  and its associated mode (m, n) is (1, 1). With the circumferential flow velocity increasing, the forward and backward travelling frequency curves meet at the point C, indicating the coupled-mode flutter.

### 3.2.1 Effects of couple forces

To analyze different stabilizing effects of couple forces  $\overline{\gamma}_{ij}$  associated with material length-scale parameter l quantitatively, critical fluid velocities by divergence are calculated, as observed from Figure 3. From this figure, critical fluid velocities when considering couple forces  $\overline{\gamma}_{ij}$  are higher than those of without couple forces  $\overline{\gamma}_{ij}$ . Compared to the shear couple forces  $\overline{\gamma}_{x\theta}$ ,  $\overline{\gamma}_{xz}$ ,  $\overline{\gamma}_{\theta z}$ , the stabilizing effects of normal couple forces  $\overline{\gamma}_{x}$ ,  $\overline{\gamma}_{\theta}$  are slightly non-significant.

The different stabilizing effects of all couple forces  $\overline{\gamma}_{ij}$  are summarized in Table 2. It is found that all couple forces do indeed influence the stability of system. The shear couple force  $\overline{\gamma}_{x\theta}$  has of the predominant stability effect while the stabilizing effect of shear couple force  $\overline{\gamma}_{xz}$  is weakest. The normal couple forces  $\overline{\gamma}_x$  and  $\overline{\gamma}_\theta$  have the same stabilizing

**Table 2:** Comparisons of dimensionless critical axial velocities instability by divergence in absence of  $\overline{\gamma}_{ij}$ ,  $\overline{\Omega}_o = 0$ ,  $\overline{U}_o = 0.006012$ .

Absence of $\overline{\gamma}_{ij}$	$\overline{\it U}'_o$	$\Delta \overline{U}'_o = \overline{U}'_o - \overline{U}_o$	$\left \Delta \overline{U}_o'\right  / \overline{U}_o'$
$\overline{\gamma}_{x}$	0.005951	-0.0000615	1.022 %
$\frac{\overline{\gamma}_x}{\overline{\gamma}_{\theta}}$ $\overline{\gamma}_{x\theta}$	0.005951	-0.0000615	1.022 %
$\overline{\gamma}_{x\theta}$	0.005143	-0.0008690	14.454 %
$\overline{\gamma}_{xz}$	0.006009	-0.0000030	0.050 %
$\overline{\gamma}_{\theta z}$	0.005993	-0.0000190	0.316 %

effects. The physical reason for the stabilizing effect induced by the couple forces  $\overline{\gamma}_{ij}$  may be given. The normal couple forces  $\overline{\gamma}_x$ ,  $\overline{\gamma}_\theta$  are regarded to be tensile axial load, and hoop load. The shear couple forces  $\overline{\gamma}_{x\theta}$ ,  $\overline{\gamma}_{xz}$ ,  $\overline{\gamma}_{\theta z}$  are considered as tensile torsion loads. The tensile couple forces strengthen the shell stiffer, thus raising the dimensionless axial flow velocities. The tensile torsion load  $\overline{\gamma}_{x\theta}$  is greater than the other loads quantitatively. Consequently, the  $\overline{\gamma}_{x\theta}$  offers the remarkable stabilizing effect. It should be noted that the couple forces may weaken the shell stiffer, which need be further studied in the future.

# 3.2.2 Effects of compound material parameter

To evaluate the different effects on the system stability induced by the shell material properties (material length-scale parameter), the new dimensionless parameter  $M_{\rm y}$  is defined.

$$M_{y} = \left(\frac{l}{r_{i}} \frac{E}{\rho_{s} g(r_{o} - r_{i})(1 - v^{2})}\right)^{1/2}$$
 (20)

here g is the gravitational acceleration.

Using the same geometric parameters and material properties in the subsection 3.2, the critical axial velocity by divergence  $U_o = 72.13 \text{m/s} \left( \overline{U_o} = 0.006012 \right)$  is obtained. The critical axial velocities by divergence induced by different factors in My are calculated and summarized in Table 3. It should to be noted that in order to get the same valve of  $M_{\nu}$ , the all factors in  $M_{\nu}$  are given certain value in the mathematical sense rather than the physical meaning. It can be seen that the effects of every factor in  $M_{\nu}$  on the system stability of are not the same. The material length-scale parameter and elastic modulus have the greater influence on the system stability than that of the Poission' ratio and shell density  $\rho_s$  for the same valve of  $M_v$ . We could modulate the main factors in  $M_{\nu}$  to control the stability of the system, which give us some insights into the designs of micro fluidshell system.

**Table 3:** Comparisons of dimensionless critical axial velocities by divergence with the same value of  $M_{\nu}$ ,  $\overline{\Omega}_{o}=0.001$ ,  $U_{o}=72.13$ m/s.

Factors in $M_{y_i}$	М <sub>у</sub> ,	$U_o' = (m/s)$	$\Delta U_o = U_o' - U_o$	$\left \Delta \overline{U}_o'\right  / \overline{U}_o'$
1×2	638.23	111.63	39.50	54.76 %
$E \times 2$	638.23	102.01	29.88	41.43 %
$\rho_s \times 1/2$	638.23	71.59	-0.54	0.75 %
$v \times 2$	642.29	68.33	-3.80	5.27 %

# 3.2.3 Coupling effect of Knudsen number and fluid viscosity

When the gap ratio k becomes smaller, the annular flow may be the slip fluid characterized by the Knudsen (Kn) number. Furthermore, the micro-scale annular flow may become a fully developed turbulent at lower Reynolds number. Considering the fluid viscosity, a shell's motion equations are modified below [24].

$$\begin{split} \frac{\partial N_{x}}{\partial x} + \frac{1}{r} \frac{\partial N_{\theta x}}{\partial \theta} + Q_{1o} \frac{\partial^{2} u}{\partial x^{2}} + Q_{2o} \frac{\partial v}{r \partial \theta} + Q_{3o} \frac{\partial^{2} u}{r^{2} \partial \theta^{2}} \\ + 2Q_{4o} \frac{\partial^{2} u}{r \partial x \partial \theta} + \frac{1}{2} \frac{\partial^{2} Y_{xz}}{r \partial x \partial \theta} + \frac{1}{2} \frac{\partial^{2} Y_{\theta z}}{r^{2} \partial \theta^{2}} = \rho_{x} \frac{\partial^{2} u}{\partial t^{2}} \end{split} \tag{21a}$$

$$\begin{split} \frac{\partial N_{x\theta}}{\partial x} + \frac{1}{r} \frac{\partial N_{\theta}}{\partial \theta} + Q_{1o} \frac{\partial^2 v}{\partial x^2} + Q_{3o} \frac{\partial^2 v}{r^2 \partial \theta^2} + 2Q_{4o} \frac{\partial^2 u}{r \partial x \partial \theta} \\ - \frac{1}{2} \frac{\partial^2 Y_{xz}}{r \partial x \partial \theta} = \rho_x \frac{\partial^2 v}{\partial t^2} \tag{21b} \\ \frac{\partial^2 M_x}{\partial x^2} + \frac{1}{r} \frac{\partial^2 M_{x\theta}}{r \partial x \partial \theta} + \frac{1}{r} \frac{\partial^2 M_{\theta x}}{r \partial x \partial \theta} - \frac{N_{\theta}}{r} + Q_{o1} \frac{\partial^2 w}{\partial x^2} \\ + Q_{3o} \left( \frac{\partial u}{r \partial x} - \frac{\partial v}{r^2 \partial \theta} + \frac{\partial^2 v}{r^2 \partial \theta^2} \right) \\ + 2Q_{4o} \left( \frac{\partial^2 w}{r \partial x \partial \theta} - \frac{\partial v}{r \partial x} \right) - \frac{1}{r} \frac{\partial^2 Y_x}{\partial x \partial \theta} \\ + \frac{1}{r} \frac{\partial^2 Y_{\theta}}{\partial x \partial \theta} - \frac{1}{2} \frac{\partial^2 Y_{x\theta}}{r^2 \partial \theta^2} + \frac{1}{2} \frac{\partial^2 Y_{x\theta}}{\partial x^2} = \rho \frac{\partial^2 w}{\partial t^2} + \rho_o \end{aligned} \tag{21c} \\ \text{in which } Q_{1o} = \frac{1 - v^2}{E h_o} \left[ -P_{xo} (x - 0.5L)^2 + 0.25 P_{xo} L_o^2 \right]; Q_{2o} = \frac{1 - v^2}{E h_o} \left[ -P_{xo} (x - 0.5L)^2 + 0.25 P_{xo} L_o^2 \right]; Q_{2o} = \frac{1 - v^2}{E h_o} \left[ -P_{xo} (x - 0.5L)^2 + 0.25 P_{xo} L_o^2 \right]; Q_{2o} = \frac{1 - v^2}{E h_o} \left[ -P_{xo} (x - 0.5L)^2 + 0.25 P_{xo} L_o^2 \right]; Q_{2o} = \frac{1 - v^2}{E h_o} \left[ -P_{xo} (x - 0.5L)^2 + 0.25 P_{xo} L_o^2 \right]; Q_{2o} = \frac{1 - v^2}{E h_o} \left[ -P_{xo} (x - 0.5L)^2 + 0.25 P_{xo} L_o^2 \right]; Q_{2o} = \frac{1 - v^2}{E h_o} \left[ -P_{xo} (x - 0.5L)^2 + 0.25 P_{xo} L_o^2 \right]; Q_{2o} = \frac{1 - v^2}{E h_o} \left[ -P_{xo} (x - 0.5L)^2 + 0.25 P_{xo} L_o^2 \right]; Q_{2o} = \frac{1 - v^2}{E h_o} \left[ -P_{xo} (x - 0.5L)^2 + 0.25 P_{xo} L_o^2 \right]; Q_{2o} = \frac{1 - v^2}{E h_o} \left[ -P_{xo} (x - 0.5L)^2 + 0.25 P_{xo} L_o^2 \right]; Q_{2o} = \frac{1 - v^2}{E h_o} \left[ -P_{xo} (x - 0.5L)^2 + 0.25 P_{xo} L_o^2 \right]; Q_{2o} = \frac{1 - v^2}{E h_o} \left[ -P_{xo} (x - 0.5L)^2 + 0.25 P_{xo} L_o^2 \right]; Q_{2o} = \frac{1 - v^2}{E h_o} \left[ -P_{xo} (x - 0.5L)^2 + 0.25 P_{xo} L_o^2 \right]; Q_{2o} = \frac{1 - v^2}{E h_o} \left[ -P_{xo} (x - 0.5L)^2 + 0.25 P_{xo} L_o^2 \right]; Q_{2o} = \frac{1 - v^2}{E h_o} \left[ -P_{xo} (x - 0.5L)^2 + 0.25 P_{xo} L_o^2 \right]; Q_{2o} = \frac{1 - v^2}{E h_o} \left[ -P_{xo} (x - 0.5L)^2 + 0.25 P_{xo} L_o^2 \right]$$

in which  $Q_{1o} = \frac{1-t^2}{Eh_o} \left[ -P_{xo}(x - 0.5L)^2 + 0.25P_{xo}L_o^2 \right]; Q_{2o} = \frac{r_o(1-v^2)}{Eh_o} P_{xo}; Q_{3o} = P_{ro}r_o; Q_{4o} = \frac{1-v^2}{Eh_o} \left[ -P_{xo}(x - 0.5L)^2 + 0.25 P_{\theta 0}L^2 \right].$ 

Here 
$$\begin{split} P_{ro} &= - \left[ \frac{2r_o}{r_o^2 - r_m^2} \right] \rho_f U_{\tau o}^2 X + 0.5 \rho_f \Omega_o^2 \left( r_o^2 - r_i^2 \right) + \\ P(0,r_o), \ P_{xo} &= \rho_f U_{\tau o}^2, \ P_{\theta o} = \rho_f v \left[ \frac{\mathrm{d} V_o}{\mathrm{d} r} - \frac{V_o}{r} \right]_{r=r_o} = \rho_f v \frac{2H}{r^2} = \\ -2 \rho_f v \Omega_o, \ v \ \text{is the dynamic viscosity of fluid.} \end{split}$$

From the Darcy formula, leading to

$$U_{\tau o}^{2} = 1/8 f \frac{r_{o}^{2} - r_{m}^{2}}{r_{o}(r_{o} - r_{i})} U_{o}^{2}$$
 (22)

f is the friction factor and the expression is given [28]

$$1/f = -1.8 \log_{10} \left[ \left( \frac{\Delta}{3.7d} \right)^{1.11} + \frac{6.9}{R_e} \right]$$
 (23)

where  $\frac{\Delta}{d}$  represents shell wall's relative roughness, while Re stands for Reynolds number.

Brighton and Jones [29] proposed the expression of  $r_m$ .

$$r_m = \sqrt{\frac{r_o^2 - r_i^2}{2 \ln(r_o/r_i)}} \tag{24}$$

Similar to Eq. (16), the shell motion equations can be rewritten through nondimensionalizing.

$$\zeta \mathbf{u} = \zeta \begin{bmatrix} \overline{u_o} \\ \overline{v_o} \\ -i\overline{w_o} \end{bmatrix} = \begin{bmatrix} 0 \\ 0 \\ 0 \end{bmatrix}$$
 (25)

Using the same material properties of shell in subsection 3.2, the geometric parameters are given

$$L=100~\mu{\rm m}, r_o=10~\mu{\rm m}, r_i=9.90099~\mu{\rm m}(k=0.01),$$
 
$$h=h_i=h_o=0.1~\mu{\rm m}.$$

The rough of shell and the fluid viscosity are given

$$\frac{\Delta}{d} = 1.4865 \times 10^{-7}, v = 1.0 \times 10^{-6} P_a \cdot s.$$

To study how the Knudsen number affects the critical flow velocity, the slip boundary conditions is used [30].

$$U_{\text{oslip}} = \text{VCF}_{\text{a}} \times U_o$$
 (26)

in which 
$$VCF_a = \left(1 + a_0 \frac{2}{\pi} tan^{-1} (a_1 Kn^B) Kn\right) \left[4 \left(\frac{2-\sigma_v}{\sigma_v}\right) + 1\right] a_0 = \frac{64}{3\pi \left(1-\frac{4}{b}\right)}, b = -1, \sigma_v = 0.7, a_1 = 4, B = 0.4 [30].$$

The results for inviscid theory are shown in Figure 4. It is found that when the Kn number is considered, the value (0.004136) of critical flow velocity by divergence decreases relative to that (0.005543) with the zero Kn number.

Similarly, Figure 5 displays the results in viscous theory. Clearly, the critical flow velocity for divergence with kn number drops by 25.39 %. For an extreme narrow annular flow, there is a larger discrepancy in the two results when considering the Kn number effect. It can also be found that fluid viscosity-induced steady viscous forces reduce the stability of fluid-mico shell system, as shown in Figure 6. To be concluded, the compound effect induced by fluid viscosity and kn number is not an ignored destabilizing factor for certain narrow annular flow. It is worthy noted that how

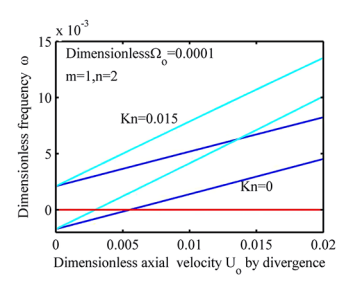


**Figure 4:** Effects of Kn number on axial flow velocities by divergence in version of inviscid theory.

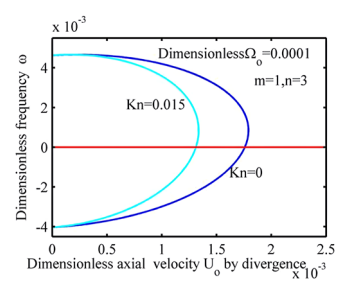


**Figure 5:** Effects of Kn number on axial flow velocities by divergence in version of viscous theory.

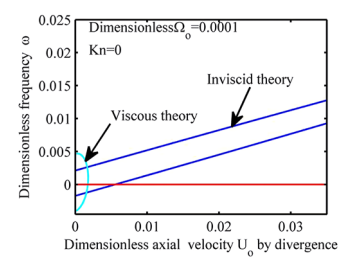


**Figure 6:** Compares of stability behaviors with/without considering fluid viscosity.

the average axial velocity correction factor is used to modify the angular fluid velocity is not provided, which deserve to further be studied.

### 3.2.4 Effects of swirling flow structure

The swirling flow is a superposition of two basic flows of Poiseuille flow and Couette flow in an annular gap. This flow has the complex flowing structure with axial fluid velocity and angular fluid velocity. Such flowing structure may come into being the complicated forces of fluid-solid interface. To characterized such flow structure, the rotation Reynolds number  $\mathrm{Re}_o = \frac{\rho_f V_o d}{2\nu}$  is introduced as well as the axial Reynolds number  $\mathrm{Re}_a = \frac{\rho_f U_{ot} d}{2\nu}$ ,  $U_{ot} = \sqrt{U_{od}^2 + U_{of}^2}$ ;  $U_{od}$ —critical fluid velocity by divergence,  $U_{of}$ —critical fluid velocity by flutter. To illustrate effects of this swirling flow structure, the ratio of the above two Reynolds numbers is defined, i. e.  $\mathrm{R}_o = \frac{\mathrm{Re}_o}{\mathrm{Re}_a} = \frac{V_o}{2U_{ot}}$  is similar to the rotation number.

Figure 7 shows the effect induced by  $R_o$  on micro-shell's stability. From this figure, it can be seen that when  $R_o$  is increased, all curves become higher. This is right because the stability of such system will be decreased with increasing of  $R_o$ . it can also be seen that when  $R_o$  gets the given valuable, stability mechanism will be changed based on the instability judgment criterion. To be concluded, the flowing structure of swirling annular flow maybe results in complex stability behaviors of such system.

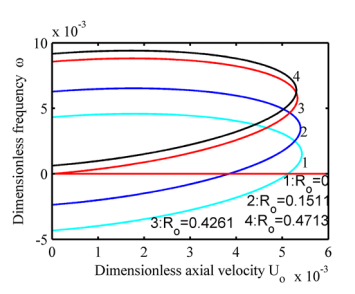


**Figure 7:** Effects of flowing structure on critical axial velocities by divergence.

# 4 Conclusions

This paper focuses on the size-dependent instability analysis on outer cylindrical shell under an annular flow involving axial and angular flow velocities on the basis of modified couple stress theory and Donnell shell theory. Both inviscid hydrodynamic pressure and viscous fluid forces can be obtained from the inviscid/viscous theories. The shell motion equations are established under the Hamilton's principle. The zero-level contour method is adopted for obtaining solutions to simply supported outer shell motion equations in travelling-wave type. The obtained findings, which are in agreement with available data, prove the proposed method feasible.

The obtained results indicate that, all the couple forces induced by the size effect can enhance the fluid-micro shell system's stability, while the stabilizing effects of the couple forces are different. The physical reason is that the tensile couple forces strengthen the shell stiffer, thus raising the dimensionless axial flow velocities. The tensile torsion couple force  $\overline{\gamma}_{x\theta}$  has of the most remarkable stabilizing effect, leading to an increase of 14.5 % in the critical velocity.

For certain narrow annular flow, we should consider the slip boundary condition which is charactered by the Knudsen number. The obtained results indicate that, the Knudsen number significantly affects the micro-shell's stability in the inviscid or viscous theory. The coupling destabilizing effect of the Knudsen number and fluid viscosity is up to 80 %, or in other words, the dimensionless critical axial flow velocity by divergence reduces from 0.005543 to 0.001311.

The obtained results indicate that, compared with the shell density and Poisson ratio, the system stability may be more likely affected by the length-scale parameter and the elastic modulus. The obtained results also indicate that, the flowing structure of swirling annular flow, presenting the ratio of rotation Reynolds number and axial Reynolds number, do affect and change the instability type of such

system. With this Reynolds number ratio increasing, the system loses stability only by flutter. It might be useful for controlling the stability by regulating flowing structures of fluid.

With this study, key findings are obtained about the stability behaviors of micro shell subjected to the swirling annular flow. These import findings are expected to guide the design and manipulate of micro devices such as micro mixer, micro head pipe, microreactor.

**Funding information:** The authors would like to gratefully acknowledge the support provided by the Huai'an Natural Science Research Plan Projects (Joint Special Projects) (No. HABL202206) and the Huai'an Kev Research and Development Projects (No. HAG202205). The authors also thank the reviewers for their valuable suggestions.

Author contribution: Wenbo Ning, Wenjian Yang: Designed and performed the experiments, analyzed the data and prepared the paper. Haoxian Wang, Kan Zhu, Yuhang Cai: Participated to collect the materials related to the experiment. Quanquan Yang, Qi Qi: Designed the experiments and revised the manuscript. All authors have accepted responsibility for the entire content of this manuscript and approved its submission.

Conflict of interest: The authors state no conflict of interest. Data availability statement: All data generated or analyzed during this study are included in this published article.

# References

- 1. Malekzadeh P, Shojaee M. Surface and nonlocal effects on the nonlinear free vibration of non-uniform nanobeams. Compos B Eng 2013;52:84-92.
- 2. Mindlin RD, Tiersten H. Effects of couple-stresses in linear elasticity. Arch Ration Mech Anal 1962;11:415-48.
- 3. Sur A, Mondal S. Effect of non-locality in the vibration of a micro-scale beam under two-temperature memory responses. Waves Random Complex Media 2022;32:2368 – 95.
- 4. Yang FACM, Chong ACM, Lam DCC, Tong P. Couple stress based strain gradient theory for elasticity. Int J Solid Struct 2002;39:2731-43.
- 5. Zeighampour H, Beni YT. Size-dependent vibration of fluid-conveying double-walled carbon nanotubes using couple stress shell theory. Phys E Low-dimens Syst Nanostruct 2014;61:28 - 39.
- 6. Sahmani S, Ansari R, Gholami R, Darvizeh A. Dynamic stability analysis of functionally graded higher-order shear deformable microshells based on the modified couple stress elasticity theory. Compos B Eng 2013;51:44-53.
- 7. Deng J, Liu Y, Zhang Z, Liu W. Size-dependent vibration and stability of multi-span viscoelastic functionally graded material nanopipes conveying fluid using a hybrid method. Compos Struct 2017:179:590 - 600.

- 8. Dehrouyeh-Semnani AM, Nikkhah-Bahrami M, Yazdi MRH. On nonlinear vibrations of micropipes conveying fluid. Int J Eng Sci 2017;117:20 - 33.
- 9. Zhu B, Xu Q, Li M, Li Y. Nonlinear free and forced vibrations of porous functionally graded pipes conveying fluid and resting on nonlinear elastic foundation. Compos Struct 2020;252:112672.
- 10. Norouzzadeh A, Ansari R. Nonlinear dynamic behavior of small-scale shell-type structures considering surface stress effects: an isogeometric analysis. Int | Non Lin Mech 2018;101:174 – 86.
- 11. Yang Y, Wang J, Yu Y. Wave propagation in fluid-filled single-walled carbon nanotube based on the nonlocal strain gradient theory. Acta Mech Solida Sin 2018;31:484-92.
- 12. Zeighampour H, Beni YT, Karimipour I. Wave propagation in double-walled carbon nanotube conveying fluid considering slip boundary condition and shell model based on nonlocal strain gradient theory. Microfluid Nanofluidics 2017;21:85.
- 13. Filiz S, Aydogdu M. Wave propagation analysis of embedded (coupled) functionally graded nanotubesconveying fluid. Compos Struct 2015;132:1260-73.
- 14. Li L, Hu YJ. Wave propagation in fluid-conveying viscoelastic carbon nanotubes based on nonlocal strain gradient theory. Comput Mater Sci 2016;112:282-8.
- 15. Wang L, Hong Y, Dai H, Ni Q. Natural frequency and stability tuning of cantilevered CNTs conveying fluid in magnetic field. Acta Mech Solida Sin 2016;29:567-76.
- 16. Ansari R, Norouzzadeh A, Gholami R, Shojaei MF, Hosseinzadeh M. Size-dependent nonlinear vibration and instability of embedded fluid-conveying SWBNNTs in thermal environment. Phys E Low-dimens Syst Nanostruct 2014;61:148-57.
- 17. Jandaghian AA, Rahmani O. Free vibration analysis of magneto-electro-thermo-elastic nanobeams resting on a Pasternak foundation. Smart Mater Struct 2016;25:035023.
- 18. Sreehari P, Gopal D, Kishan N, Venkadeshwaran K, Singh S, Karthik K. A numerical study on the radiative flow of magneto-Casson fluid via a vertical microchannel with entropy generation. J Kor Phys Soc 2025;86:372 - 82.
- 19. Munjam SR, Gopal D, Kishan N, Formanova S, Karthik K, Ahmad F, et al. Brownian motion in a magneto Thermo-diffusion fluid flow over a semi-circular stretching surface. Part Differ Equ Appl Math 2024:12:100970.
- 20. Bashettahalli Ranganath K, Hosahalli Marulappa S, Bannihalli Naganagowda H, Allabaksh S, Muhammad T, Yeliyur Honnappa G, et al. Investigation of squeeze film characteristics between a sphere and a flat plate in the presence of porous medium: rabinowitsch fluid model. ZAMM - J Appl Math Mech 2025;105:e70015.
- 21. Thompson PA, Troian SM. A general boundary condition for liquid flow at solid surfaces. Nature 1997;389:360 – 2.
- 22. Wang K, Chai Z, Hou G, Chen W, Xu S. Slip boundary condition for lattice Boltzmann modeling of liquid flows. Comput Fluid 2018;161:60 - 73.
- 23. Neto C, Evans DR, Bonaccurso E, Butt HJ, Craig VS. Boundary slip in Newtonian liquids: a review of experimental studies. Rep Prog Phys 2005;68:2859-97.
- 24. Ning WB, Gao R, Li Y, Wang S. Size-dependent stability analysis of a functionally graded cylindrical shell subjected to swirling annular flow including the fluid viscosity. Ocean Eng 2021;224:108755.
- 25. Amabili M. Nonlinear vibrations and stability of shells and plates. New York: Cambridge University Press; 2008.

- 26. Zhou X, Wang L. Vibration and stability of micro-scale cylindrical shells conveying fluid based on modified couple stress theory. Micro Nano Lett 2012;7: 679-84.
- 27. Zhang XM, Liu GR, Lam KY. Coupled vibration analysis of fluid-filled cylindrical shells using the wave propagation approach. Appl Acoust 2001;62:229-43.
- 28. Haaland SE. Simple and explicit formulas for the friction factor in turbulent pipe flow. J Fluid Eng 1983;105:89-90.
- 29. Brighton JA, Jones JB. Fully developed turbulent flow in annuli. J Fluid Eng 1964;86:835-42.
- 30. Mirramezani M, Mirdamadi HR. The effects of Knudsen-dependent flow velocity on vibrations of a nano-pipe conveying fluid. Arch Appl Mech 2012;82:879-90.